Available online at www.sciencedirect.com
SCIENCE DIRECT®
ELSEVIER
Applied Surface Science 214 (2003) 319–337
applied surface science
www.elsevier.com/locate/apsusc

Characterization of PdAu thin films on oxidized silicon wafers: interdiffusion and reaction

Senay Yalcin[a], Recep Avci[b,*]

[a]*Fen Edebiyat Fakultesi, Bahcesehir Universitesi, Istanbul, Turkey*
[b]*Department of Physics, Montana State University, EPS 264, Bozeman, MT 59717, USA*

Received 8 August 2002; received in revised form 8 August 2002; accepted 11 March 2003

Abstract

Plasma-deposited thin films prepared at room temperature, ranging from 46 to 250 Å of PdAu on ~45–50 Å Si-oxide and Si-oxynitride films grown on Si wafers were studied. Grazing incidence X-ray diffraction, X-ray reflectivity, and XPS depth profile techniques were used to characterize the thin films. A reactive interface involving Pd- and Au-silicides is formed, linking the thin film to the Si-oxide and Si-oxynitride films: a small fraction of Pd and Au atoms from PdAu migrate into the Si substrate, first penetrating the oxide layer, and the small fraction of Si atoms from the oxide layer migrate into the PdAu film and form a silicide interlayer consisting of a reactive interface made up of mixtures of Au- and Pd-silicides interspersed within the matrix of PdAu and substrate. The concentration profiles of these silicides have a maximum at the interface with decay on both sides. The density and the face-centered cubic (fcc) lattice parameter of the film are determined to be $\sim 13 \pm 1$ g/cm^3 and $\sim 4.004 \pm 0.014$ Å, respectively. The ideal film density is expected to be ~15.5 g/cm^3, which suggests substantial defect density and light material mixture, causing more than 13% reduction in the mass density of the film.

PACS: 68.35.-p; 68.35.Fx; 79.60.-i; 61.10.Kw; 61.10.Yh

Keywords: PdAu thin films; PdAu/SiO_2/Si; Silicide; Interdiffusion and reaction; XPS; Reflectivity

1. Introduction

PdAu films have received substantial interest in recent years for their potential in catalysis [1–3] and fuel-cell applications [4]. For example, in the hydrogenation reaction of acetylene in ethene, the presence of Au reduces hydrocarbon poisoning and improves the catalytic activity and selectivity of PdAu on a silica-supported substrate [1]. Similarly, the electrocatalytic activity of PdAu with respect to CO tolerance was shown to be superior to that of the best PtRu catalyst [4]. Our motivation for this work was to understand the thin film properties of the PdAu alloys commonly used for their small grain size (<20 Å) in scanning electron microscopy (SEM) as conducting coatings of insulating samples. The particular question of interest was to determine the true thickness and defect density of these conducting thin films and, hence, to determine the true mass density of the film deposited on the insulating materials. Such information is needed in order to assess the amount of X-rays absorbed as the X-rays pass through the thin film [5].

* Corresponding author. Tel.: +1-406-994-6164; fax: +1-406-994-6165.
E-mail address: avci@physics.montana.edu (R. Avci).

0169-4332/03/$ – see front matter © 2003 Elsevier Science B.V. All rights reserved.
doi:10.1016/S0169-4332(03)00519-1

These characteristic X-rays are typically generated within the insulating material under investigation via focused high-energy electrons of ∼15–30 keV energy. Typically, PdAu films of ∼100–150 Å are used for such applications. For simplicity, it was decided that a flat silicon wafer with a reasonably thick (40–50 Å) oxide layer would be a good substrate. Some of the best techniques for determining the thickness and mass density independently are X-ray reflectivity and grazing incidence X-ray diffraction. The interactions of Pd and Au with clean Si surfaces are well known. Because of the thick oxide or oxynitride barriers such interactions would be minimal. However, this assumption turns out to be incorrect as explained below: some small fraction of Si atoms from the substrate and some Pd and Au atoms from the PdAu (actually, Pd_xAu_{1-x} with $x \sim 0.53$) thin film migrate into each others' regions and establish a reactive interface consisting of Pd and Au silicides intermixed with the PdAu and Si-oxide or Si-oxynitride matrices. A Si-oxide (SiO_2) or nitrided Si-oxide film (referred to herein as Si-oxynitride) of ∼45–50 Å on Si substrate does not prevent Au–Si or Pd–Si reactions or the migration of constituent atoms from one region into the other.

A large number of studies involving Pd or Au overlayers on various Si surfaces, or Si overlayers on various Pd and Au surfaces, have been reported. The common theme in all of these studies is that both Au and Pd interact with the surface and form silicides. Several groups [6–10] studied the interaction of Au with well-characterized Si surfaces. For example, studies of Au films on Si(1 1 1) surfaces show that Si segregates on top of the deposited gold film whether the Si(1 1 1) surface is a clean (7 × 7) structure or an H-terminated (1 × 1) structure [6]. No intermixing of gold and silicon is reported for Au films of a couple of monolayers on Si surface. In [11], the authors report high-resolution transmission electron microscopy (HRTEM) studies of Au films on atomically clean Si(1 0 0) and Si(1 1 1) surfaces. They notice a distinct difference in interface formation between the two surfaces. Cross-section analysis using HRTEM on 400 Å of gold film deposited on atomically clean Si(1 0 0) surface at room temperature shows the formation of a discontinuous amorphous interlayer which has a thickness of about 35–40 Å. In situ reflection high-energy electron diffraction (HREED) analysis confirms the existence of Au–silicide formations of Au_4Si stoichiometric composition. The interface between the interlayer and the Au film was observed to be rather rough due to appreciable intermixing during deposition. Similar studies conducted on Si(1 1 1) surface show no amorphous silicide interlayer and hence no mixing between the Au and Si [10]. However, the Auger electron spectroscopy (AES) and scanning tunneling microscopy (STM) studies on Au films on H-terminated Si(1 1 1) surfaces show pronounced migration of Si atoms into an Au overlayer at least 50 Å thick [12]. AES studies on systems involving the deposition of Si overlayers on Au surfaces also show diffusion of Si into the Au substrate [13]. The early stages of Au coverage on Si(1 1 1)-7 × 7 surface are reported in [14], where Au adsorption appears to be coverage-dependent. The latter reference has a reasonable bibliography of Au/Si systems.

Though it is not clear why Au should have different interactions with different Si surfaces, gold has been known to react with Si surfaces very strongly even below room temperatures, as the above examples indicate. The measure of such an interaction can be determined from chemical shifts observed in the Au core levels as compared to their value in the metallic state. In [15], the authors report shifts up to 1.2 eV toward the higher binding energy in the Au 4f lines upon the formation of Au-silicides. A UHV study using high-resolution electron microscopy and chemical analysis of Au overlayers on Si(0 0 1) surface in [16] emphasizes the role of the surface growth and morphology in the relative core level shifts observed in XPS and AES.

Palladium, like gold, forms a reactive layer on Si. Transmission electron microscopy (TEM) and X-ray diffraction (XRD) studies on 300 Å Pd films deposited at room temperature on Si(1 1 1) substrate show Pd_2Si silicide formation [17]. These latter studies were not conducted in a UHV environment, and the samples most likely had native oxide formations on them. The fact that silicide formations are observed with XRD and TEM to coexist with the unreacted Pd suggests, on purely fundamental reasoning, that considerable diffusion and reaction are taking place in the interface at and above room temperatures.

Experiments using LEED and STM conducted on Pd(1 0 0) surface exposed to silane chemical vapors show amorphous palladium–silicide/silicon interface

formation [18], in which Si is incorporated into the Pd surface. Similar studies using IR and STM on Si/Pd(1 1 0) and Si/Pd(1 0 0) systems conclude that the nucleation and growth of silicide formation upon Si deposition on Pd are similar to the silicide formation upon Pd deposition on Si substrate [19–21]. The Si/Pd interface is extremely reactive, and silicide reaction occurs at $T \leq 180$ K; at room temperature amorphous silicide dominates. The amorphous silicide films are proposed to have a non-uniform chemical composition, in that Si clusters are randomly intermixed in the silicide film, having a Pd_2Si stoichiometry.

Reflectivity studies can determine electron density and the thickness of the thin film independently [22–28]. The X-rays incident on a multilayer system will reflect according to Fresnell reflectivity if the surface is ideal with no roughness. In most cases the roughness of the reflecting surface is comparable to the X-ray wavelength. This means that the reflection from these surfaces is usually less than that predicted by Fresnel reflectivity. The difference can be attributed to the surface and interface roughness [24,25,29]. The combination of reflectivity and glancing incidence X-ray diffraction is a powerful technique for determining both the crystal structure and the thin film properties in one measurement. The nanometer-scale epitaxial structure, morphology, and surface and interface roughness in principle can be determined using such a combination [24,25,29,30].

Not much has been reported on Au or Pd overlayers or their interactions with the oxide-covered Si substrate. In their work on the characterization and catalytic activity of the $PdAu/SiO_2$ system, Juszczyk et al. [3] report that the formation of Pd-silicides at the interface acts as a *chemical glue* between the PdAu catalyst and the silica support. An X-ray reflectivity and STM study of sputter-deposited Au films on native oxide-covered Si substrate was reported in [31]. The latter does not comment on the interface roughness; instead it focuses on the top layer of the Au surface. Our experience in this work is that specular reflectivity results are not too sensitive to interface roughness in the models used. Off-specular reflection is better suited to interface roughness analysis [27]; hence, it is not surprising that the specular reflectivity measurements on the Au/Si system reported in [31] could not resolve the chemical and physical roughness in the interface.

The study of Pd on Au serves as a reference system, particularly in relation to the XPS core line positions of Au and Pd. Once a Pd/Au layer is deposited on a Si substrate, the interdiffusion of Si atoms and subsequent chemical reactions cause chemical shifts as well as line profile changes in the core levels of the atoms involved. The work on thin films of Pd on Au(1 1 1) reported in [32] is helpful here: PdAu alloy formation takes place at room temperature and very small shifts in the Au 4f and Pd 3d core levels are observed ($\leq$0.2 eV) as a function of coverage and the annealing temperature. In this work, we report drastic changes in the line profile and peak positions. We attribute all of these changes to the interaction of Pd and Au with Si in the mutual environment of the constituent atoms.

2. Experimental

The experiments were performed at the Image and Chemical Analysis Laboratory (ICAL) [33] at Montana State University, using a Scintag X-ray diffraction (XRD) system and a Physical Electronics 5100ci XPS system. In the XPS studies monochromatized Al Kα X-rays were used. The analysis area of the sample was $\sim$0.8 mm in diameter, while the sputter area was 3 mm $\times$ 3 mm. The majority of our studies involved depth profiling, employing a differentially pumped Ar-ion gun operating at $\sim$2 keV (in some cases at $\sim$3.5 keV) energy with ion currents not exceeding 0.45 μA. Typically a depth-profile cycle involves

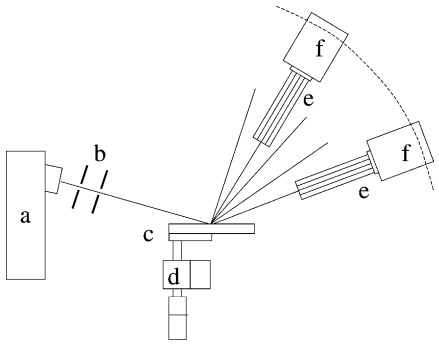

Fig. 1. Schematics of the XRD system used for specular X-ray reflectivity and grazing-incidence X-ray diffraction studies: (a) X-ray source; (b) beam defining slits; (c) thin-film substrate; (d) micro-manipulator for adjusting the sample height; (e) soller slits; and (f) Ge solid-state X-ray detector.

acquiring a number of core level spectra around the preselected core regions (*multiplex cycle*). During this period no sputtering is done. (The high voltage to the Ar-ion gun is turned off.) Following the multiplexing, the system stops acquiring spectra and the *sputter cycle* starts by applying an accelerating voltage to the Ar-ion gun for a predetermined amount of time. The combination of a multiplex and a sputter event generates a single cycle, which generates a single data point (such as core level and peak intensity value) used in the sputter-depth profile of each of the elements under consideration. Electrons are collected at 45° emission, and the spherical-sector-analyzer pass-energy is selected (typically ∼58.7 eV) for optimum signal-to-noise ratio and energy resolution. Core line fits were done using *PHI Access* software to separate the chemically related peaks associated with Au- and Pd-silicide reactions as well as the Si-oxide and Si

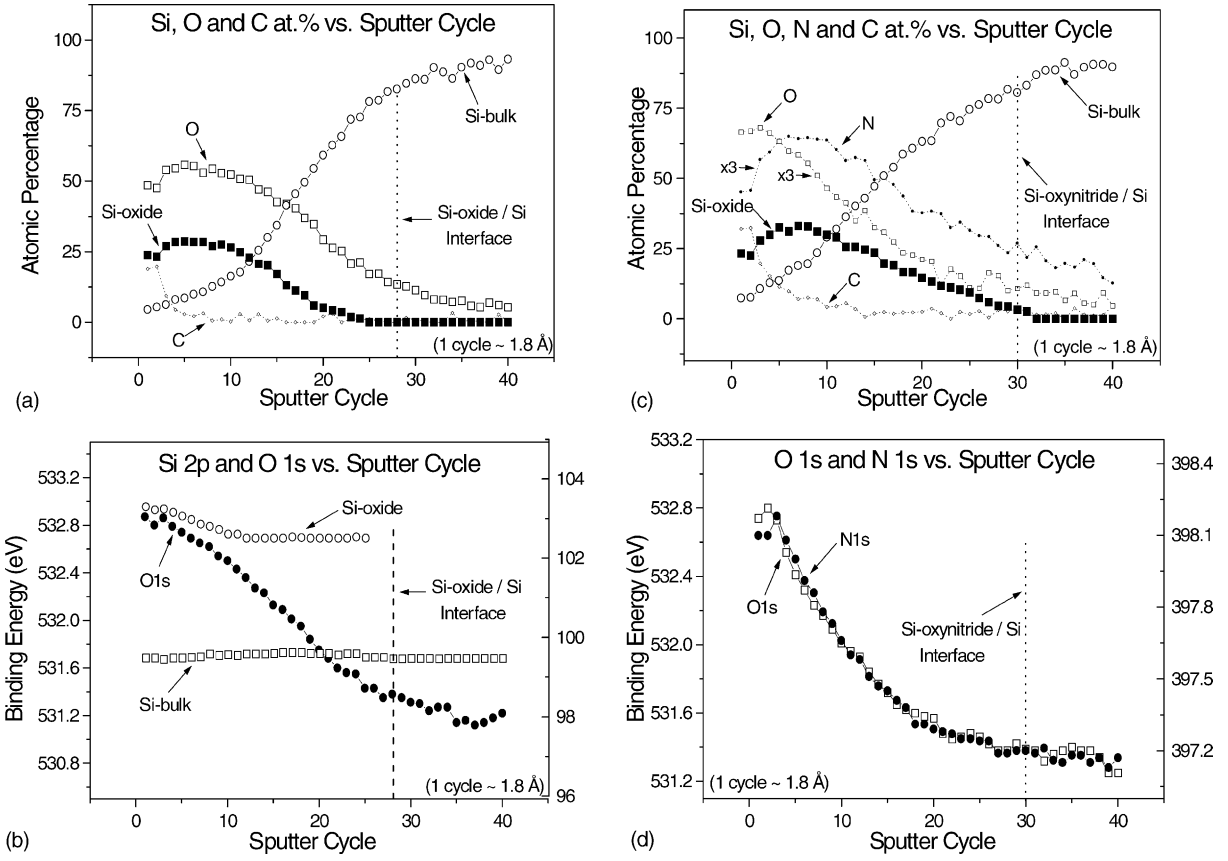

Fig. 2. (a) Atomic concentrations of O, C, and Si (separated into oxide and bulk components) as a function of sputter cycle. In all figures the oxide/bulk interface is marked as a vertical dash line; (b) the O 1s and Si 2p (separated into oxide and bulk components as in the inset of Fig. 7c) core line positions as a function of sputter cycle. The scale on the right-hand side goes with the Si 2p line. In the experiments described here each sputter cycle removes ∼1.8 Å of material. The substrate described in (a) and (b) is used for the thin film experiments associated with Figs. 3–7. The substrates described in figures (c) and (d) are used in the thin film experiments described in Figs. 8 and 9a and c and a very similar (to the latter) substrate is used for the experiments described in Figs. 9b and 10; (c) atomic concentrations of Si, O, N and C as a function of sputter cycle. The Si-oxynitride (SiO_xN_y)/Si-bulk interface position is marked with a vertical dashed line; (d) the O 1s and N 1s as a function of sputter cycle. The scale on the right-hand side goes with the N 1s line. The oxynitride thickness of the film described in (c) and (d) is about ∼51 Å. The oxide thickness described in (a) and (b) is ∼46 Å. Note that the O 1s line is decreasing, but the same is increases by as much as 1.7 eV (see Fig. 9a) in the presence of the PdAu film deposited on the oxide dielectric. This is interpreted as PdAu film interacting with the oxide or oxynitride film. Also notice that the Si concentration described in (a) is slightly different from that shown in Fig. 7d. This gives further support to the conclusion that PdAu is interacting with the oxide film as discussed in the text.

bulk peaks. In these fittings care was taken to maintain consistent peak width and peak positions, paying attention to the relation between the spin-orbit-split peaks. The peak widths used in the fits were determined by measuring the Au and Pd core lines corresponding to pure PdAu alloy and pure Au- and Pd-silicides before we began and after we finished the sputtering cycles, respectively. For silicides, due to their asymmetric peak profiles, the peak heights were used instead of the areas under the peaks to separate the Au- and Pd-silicides from the PdAu component. This is because the peak heights were less sensitive to the slight variations in the peak profiles in the peak fitting routines. In all other quantitative analyses the areas under the peaks were used to represent the concentration profiles.

The XRD set-up was operated in thin-film analysis mode, using a Cu Kα line as the X-ray source. A special sample holder was constructed for thin-film studies allowing sample-height adjustments to accuracy within a micron; plus, a special thin-film attachment (a set of soller slits) was used in front of the solid state detector. All thin-film XRD measurements were carried out at incident X-ray angles varying between 0.1° and 2.0°. A large area, at least 1 cm × 1.5 cm, was analyzed. XRD studies were conducted in two modes: the reflectivity and the grazing incidence X-ray diffraction modes. All the reflectivity studies were conducted in the specular reflection configuration, while the grazing incidence diffraction studies were conducted with 2θ not exceeding 60°. A schematic of the modified XRD system is shown in Fig. 1. The X-ray reflectivity data were analyzed using reflectivity software freely accessible at http://www-cxro.lbl.gov/optical_constants/.

It was important for the Si wafers used to have a reasonably thick oxide layer to prevent cross reactions with bulk Si, and to be reasonably flat so that thin-film reflectivity and diffraction experiments could be performed. Atomic force microscopy (AFM) with a Digital Instruments Dimension 3100 system was used to assess the surface roughness of the Si wafers and that of the PdAu thin films. The surface roughnesses, R, defined as $R = \sqrt{\sum_{i=1}^{N}(Z_i - Z_{\text{ave}})^2/N}$, where Z_i is the surface height at position i, and Z_{ave} the average surface height, were determined before and after the thin-film depositions, which yielded ∼5 Å and 10–15 Å, respectively. Si wafers were oxidized either by rapid thermal heating in an oxygen atmosphere at ∼1100 °C or by heating in a NH_3 atmosphere at ∼1100 °C (oxynitride formation). All wafers used were in the (1 0 0) orientation. The quality of the surface flatness was very important for the reflectivity measurements. Several low-grade commercial Si wafers available in our laboratory did not produce acceptable reflectivity curves due to excessive surface roughness. The Si-oxide and Si-oxynitride films were analyzed and are described below; relevant literature on the nature of these films can be found in [34–41]. These oxides were characterized using XPS depth profiling as shown in Fig. 2 described in Section 3 below.

The substrates were cleaned before thin-film deposition by sonicating first in acetone, then in hexane, and finally in methanol; this was all done in ambient conditions. Thin films of PdAu alloy were deposited, using the standard procedure, in a 133 mbar Ar atmosphere employing a commercial plasma-deposition system (Hummer VII from Anatech, Ltd.) used for coating the insulating samples for analysis in the scanning electron microscope. The PdAu target (7.6 cm diameter) used in the coater was also purchased from Anatech, Ltd. The substrate was kept at room temperature during deposition and analysis. The sputter specifications are such that during deposition the sample was not exposed to plasma ions of any kind; neither was it exposed to any secondary energetic particles. Metal atoms sputtered off of the target are thermalized as they disperse through the process chamber before arriving at the surface. The company specification of the grain size of the thin films is better than 20 Å [42], which agreed with the AFM roughness measurements. The samples were not cleaned after the thin-film deposition but kept in clean containers in ambient conditions. XPS analysis was performed 2 months after the preparation of the thin films.

3. Results

3.1. XPS studies

Most of our XPS studies involve depth profiling as described above, though some involve angular-dependent XPS studies as presented below. Each substrate

with or without a thin film of PdAu alloy deposited on oxidized Si wafer was introduced into the ultra-high vacuum (UHV) chamber at ∼6–7 × 10^{-10} mbar pressure, and was subjected to a cycle of sputter and XPS analysis. A complete core level spectrum of each region under consideration was stored in each cycle of analysis. For example, a 32-cycle study produces 128 spectra. These spectra contain both the core level position and the intensity information as a function of sputter cycle. A low-energy electron flood gun was used to compensate charging.

XPS depth profile experiments were conducted on the Si-oxide and Si-oxynitride films with no PdAu films on them. It is important to emphasize here that these samples were taken from the other halves of the wafers used for thin-film deposition. These data are presented in Fig. 2a–d. The Si-oxide and Si-oxynitride thicknesses were determined to be ∼46 and 51 Å, respectively, using a method similar to that described in [43,44], in which the noninvasive technique is used of taking the ratio of the oxide to the bulk components of the Si 2p peak intensities at 45° emission angle. Though the spirit of the approach of determining the oxide thickness is the same as in [44], we developed this technique for a different application independent of [44], in that we also took the acceptance angle of the analyzer into account in our analysis. The results of the Si-oxide sputter-depth profile analysis are shown in Fig. 2a and b. These data were taken using an Ar-ion beam at ∼2 keV energy at 0.25 mA current. Note that the O 1s line position decreases with increasing sputter cycle, but increases with increasing sputtering by as much as 1.7 eV (see Fig. 9a) in the presence of the PdAu film deposited on the oxide dielectric. This is interpreted as PdAu film interacting with the Si-oxide or Si-oxynitride films as discussed later in the text.

Fig. 3 shows the XPS spectra around the Au 4f region as a function of sputter cycles from 1 through 32. The thickness of the PdAu film was about 46 Å as determined by the reflectivity measurements presented below (Fig. 12). The PdAu thin film was deposited on ∼46 Å Si-oxide grown on a Si wafer. No sputtering was done (per software instructions) between cycles 1 and 2, and the sputtering started at the end of cycle 2. Each cycle of sputter removes ∼4 Å of material from the surface using Ar^+ ions at about 3.5 keV energy at 0.4 μA current. Later these experiments were repeated with ∼2 keV Ar ions at ∼0.3 μA current to check for possible beam-mixing, which could not be verified. (The results were identical.) The peak shown at ∼100 eV in the figure is the bulk Si 2p peak, which marks the region where Si bulk becomes visible. Similarly, Fig. 4 shows the XPS core

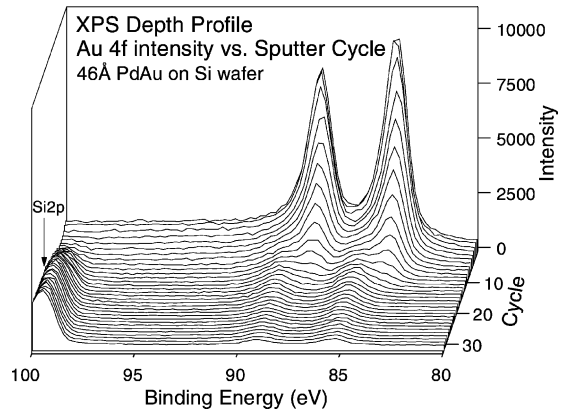

Fig. 3. Au 4f vs. sputter cycle for a ∼46 Å PdAu film sputter-deposited on a ∼46 Å Si-oxide film grown on Si(1 0 0). The sputtering starts after cycle 2. The peak around 100 eV corresponds to the bulk Si 2p peak. Note that Au core lines suffer a chemical shift (∼1.5 eV increase) and this component of the 4f line dominates with increased sputtering. This shift is attributed to the formation of Au-silicides (see text for details). Notice that Au diffuses into the Si bulk as suggested by the non-zero peak intensity at cycle 32.

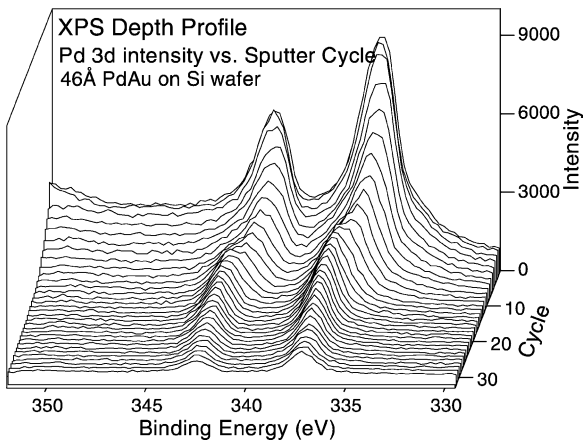

Fig. 4. Pd 3d vs. sputter cycle for the system described in Fig. 3. As in Au 4f the observed chemical shift in the Pd 3d line is attributed to Pd-silicide formation. Note also that the relative (to unsputtered cycle) Pd peak intensity at cycle 32 is higher than that of Au 4f at cycle 32, indicating that substantial Pd inter-diffusion is taking place into the Si-substrate.

level spectra for the Pd 3d levels as a function of sputter cycle from 1 through 32 as described above. A careful examination of Figs. 3 and 4 shows the formation of silicides involving a small fraction of thin film and substrate atoms spreading into the thin film and into the substrate as explained in Section 4 below.

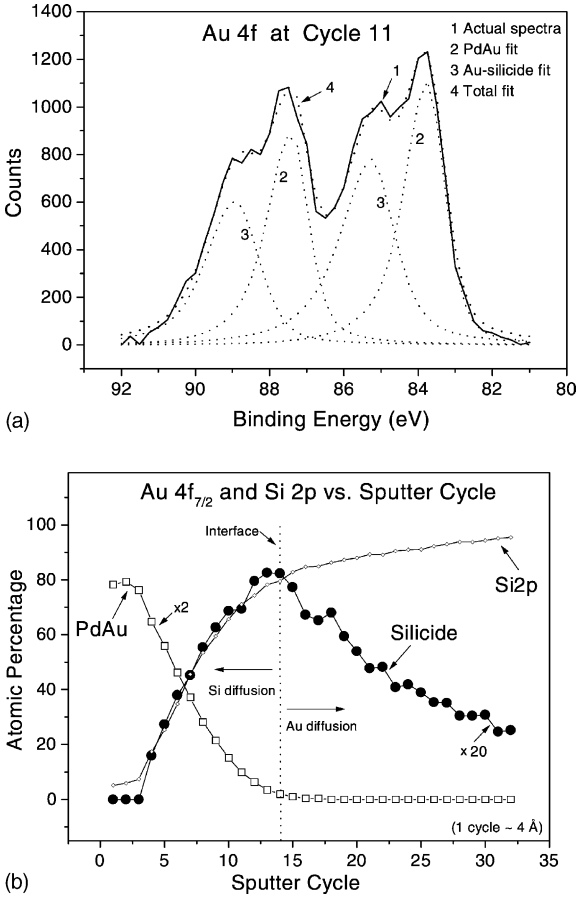

Fig. 5. (a) Au 4f spectra taken at cycle 11. Notice two distinct peaks for each of the spin-orbit-split lines. The peak marked as 1 is the actual spectrum, and the dotted lines are the peak fits as described in the text. The pair labeled as 2 is assigned to Au 4f in AuPd alloy while the pair labeled as 3 is assigned to Au 4f in Au-silicide. The profile labeled as 4 is the total fit; (b) Au 4f and Si 2p peak intensity vs. the sputter cycle. Au $4f_{7/2}$ has been separated into two components as shown in (a): the component associated with PdAu (peak 2 in (a)) and the other with Au-silicide (peak 3 in (a)). Depending on the height of these peaks the Au 4f intensity is partitioned into two components: open squares represent Au concentration in PdAu environment; full circles, in Au-silicide environment. Open diamonds give the Si concentration. Each cycle starting from cycle 2 corresponds to ~4 Å of depth. The dashed vertical line shows the PdAu/Si interface, and the arrows indicate the direction of the migrations for the appropriate atoms. The concentrations are normalized such that the Pd, Au and Si concentrations all add up to 100%. This is also the case in Fig. 6b.

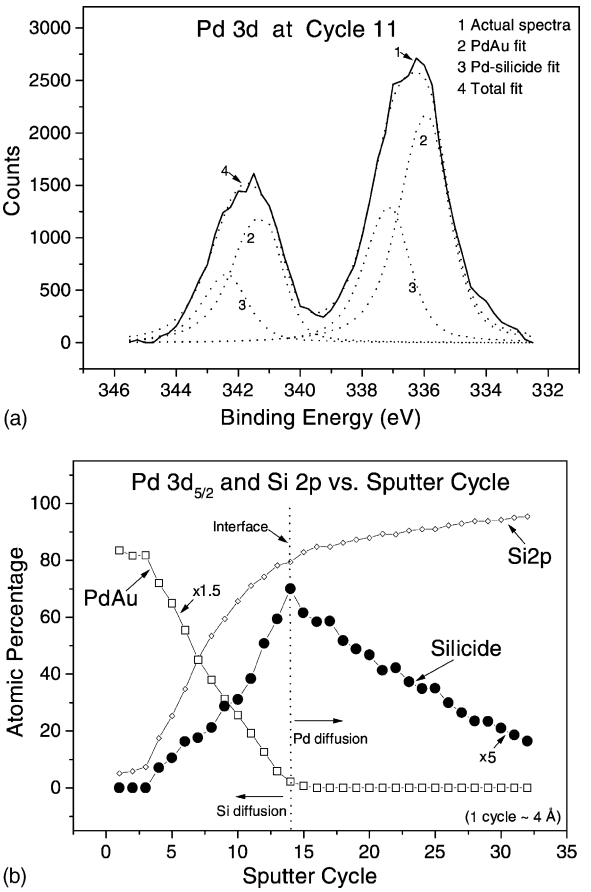

Fig. 6. (a) Pd 3d spectra (like Fig. 5a) taken at the 11th cycle. The full line is the actual spectrum, the dotted lines are the peak fits, and the profile labeled as 4 is the total fit. The Pd peak fitting was slightly more challenging than the Au. The widths and the relative intensity ratios of the peaks associated with the individual pairs labeled as 2 and 3 were determined from the spectra taken at cycles 1 and 32, respectively. In some cases we noticed a clear shoulder, which made fitting easier. The doublet labeled as 2 is assigned to Pd 3d in PdAu alloy, and pair 3 is assigned to Pd 3d in Pd-silicide formation; (b) this is very similar to Fig. 5b except this time we plot Pd and Si concentration vs. the sputter cycle. As explained in Fig. 5b, the Pd 3d is separated by means of peak fitting into PdAu and Pd-silicide components. Full circles show the behavior of the Pd-silicide, open squares represent the Pd 3d in PdAu environment, and the Si concentrations are shown for reference. Again, the vertical dashed line marks the PdAu/Si interface, where PdAu components of Pd and that of Au cease to exist. Horizontal arrows show the direction of diffusion for Pd and Si.

Figs. 5a and 6a show typical core level spectra corresponding to the Au 4f and Pd 3d lines, respectively, obtained at the 11th cycle, ∼35 Å into the PdAu film. The full lines are the actual spectra, while the dotted lines are spin-orbit-split fits. The full width at half maximum (FWHM) and line profiles of the individual peak components are obtained from similar fits corresponding to the pure AuPd at cycle 1 and pure Au- and Pd-silicides at the end of cycle 32. The spin-orbit intensity ratios as well as the peak splittings were maintained in the peak fitting. Each core level peak associated with Au and Pd has two components: the component associated with AuPd alloy and the component associated with Au- and Pd-silicide formation. The Au 4f level shifts up by ∼1.5 eV; the Pd 3d level, by ∼1.8 eV; as compared to the PdAu values (Fig. 7a and b). No attempt is made to separate the Si in the Pd- and Au-silicide from the Si in the oxide or bulk environments. In [15], the authors study the Si 2p core line changes in the Au-silicide environment and assign the position at ∼101 eV to the Si 2p component in the Au-silicide environment. The suboxides of Si in

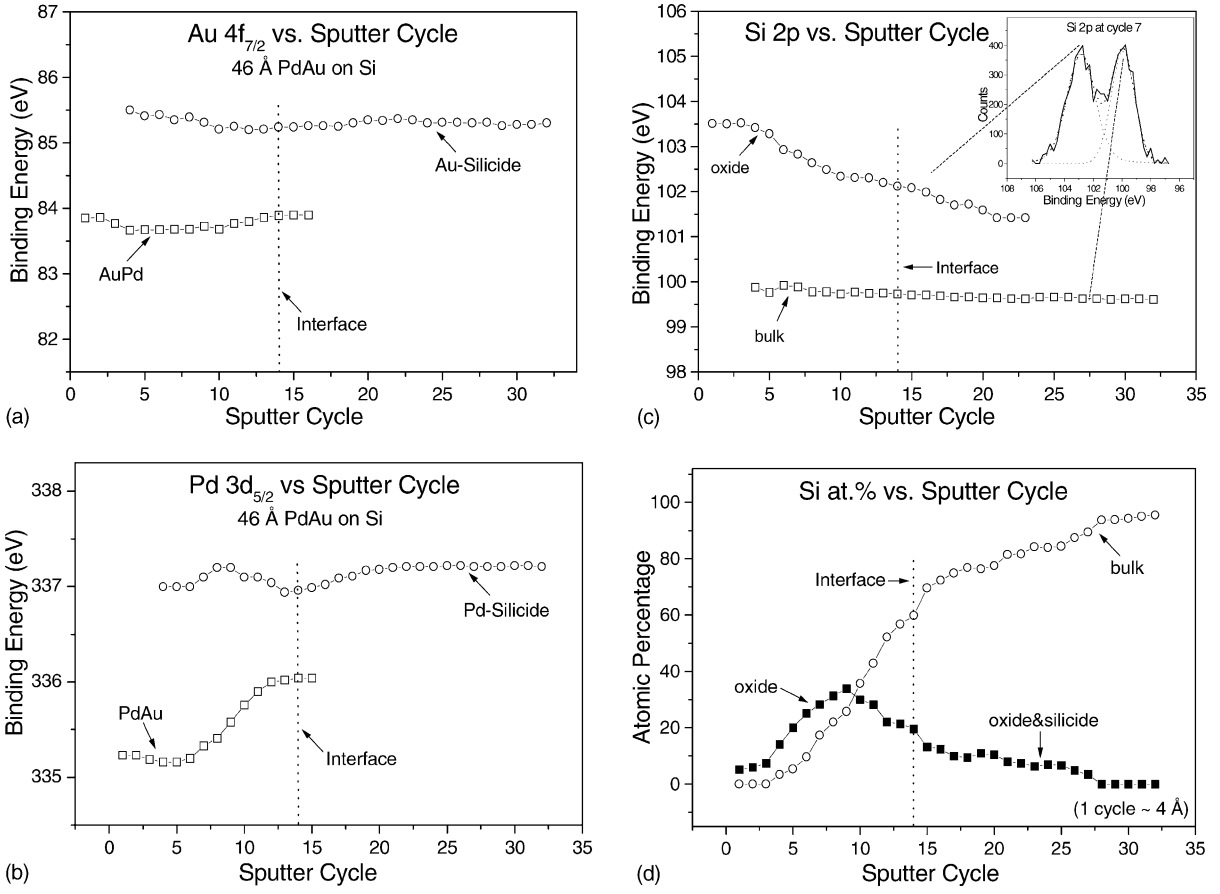

Fig. 7. (a) Au $4f_{7/2}$ vs. sputter cycle corresponding to Fig. 3. Here again, peaks are separated into AuPd and Au-silicide components as described in Fig. 5a. The horizontal line marks the interface as in Figs. 5 and 6; (b) Pd $3d_{5/2}$ vs. sputter cycle, corresponding to Fig. 4. The components corresponding to PdAu and Pd-silicide as described in Fig. 6b vs. the sputter cycle show slight variations in Pd-silicide position, most likely due to imperfections in the peak fitting routine, but show a major increase in the position corresponding to PdAu component as a function of sputter cycle; (c) Si 2p vs. sputter cycle. Oxide and bulk components are separated as shown in the inset, which corresponds to Si 2p at the 11th cycle. The dotted lines in the inset correspond to peak fittings. No attempt is made to separate the silicide component. The variations in the oxide position as a function of sputter cycle are related to sputter-induced reduction of the oxidation state of Si; (d) Si 2p concentrations vs. sputter cycle. The peak intensities are separated into *oxide* and *bulk* components as shown in the inset (c); the concentrations are normalized as described in Fig. 5b. The vertical line marks the interface position.

the SiO_x environment [35,38] interfere with this assignment. Similar difficulties are encountered in our analysis.

Figs. 5b and 6b show the variations in the core level peak intensities (in percentages) as a function of sputter cycle. Here, the areas under the Au, Pd and Si peaks are normalized to add up to 100%. The Au and Pd percentages are split into two parts: one for the AuPd alloy and the other for the Au- and Pd-silicides. The lever-rule is used to split the percentages, so that a given Au or Pd percentage is split in proportion to the peak heights of the individual components determined using the peak fitting routines described in Figs. 5a and 6a. From the analysis of the peak intensities we conclude that the PdAu/Si interface is located at about the 14th cycle, which is marked as a vertical dashed line in Figs. 5b and 6b, where the PdAu components of the Au and Pd diminish while the silicide components reach their maximum. We assigned the ∼46 Å thickness to the first 14 cycles of sputtering. The location of the interface has some uncertainty due to interface roughness. Cycle 12 or 13 can equally be assigned as the interface. It appears that at the interface the silicide concentration reaches a maximum, which makes sense from the statistical point of view. Assigning precise locations in depth profiling is complicated by the fact that photoelectrons arriving at the analyzer from the Au 4f, Si 2p and Pd 3d core levels at kinetic energies ∼1400, 1385, and 1150 eV, respectively, have finite penetration depths and are sampling deeper into the surface with an exponential decay. The attenuation lengths of these electrons are ∼10–25 Å, depending on the material in which they move [45].

If one examines the behavior of Si, Au and Pd in terms of inter-diffusion and reaction one notices that a small fraction of Si inter-diffuses almost to the top of the PdAu film, forming Au- and Pd-silicides, which are interspersed within the PdAu thin film. Similarly, we notice that small fractions of Pd and Au inter-diffuse into the Si oxide (∼45–50 Å thick), and then proceed to move into the Si bulk. The Pd appears to diffuse more readily than the Au, as is seen in comparing the scales of the intensity distribution curves in Figs. 5b and 6b (also see Figs. 3 and 4), where we marked the direction of migration of Si, Au and Pd atoms with horizontal arrows. In both figures Si intensity is shown for reference.

Variation in the Au, Pd and Si core level positions is shown as a function of sputter cycle in Fig. 7a–c. Notice that the Au 4f (AuPd and Au-silicide) and Si 2p levels associated with the Si bulk do not change much as a function of sputter cycle, but that the Si 2p level associated with the Si oxide decreases with increased sputtering. The Pd 3d level in PdAu phase increases substantially with increased sputtering. However, the Pd 3d associated with Pd-silicide does not show much variation. The role of oxygen and nitrogen have not been discussed in these studies, partly because we do not understand it and how it relates to the rest of the interactions under study, and partly because we do not know the role, if any, of the ambient oxygen in any of these studies. Since our samples were not atomically clean there was always some oxygen in the system (see Fig. 8c also) even though no deliberate attempt was made to expose the thin films to the oxygen. In Fig. 7d, we separate the Si intensity into the bulk and the oxide components as shown in the inset in Fig. 7c, and mark the interface position in the figure. If Fig. 7c is compared with Fig. 7a and b, it is clear that the oxide component of Si 2p extends beyond the line marking the location of interface. This is used to resolve an apparent contradiction in locating the oxide film relative to the PdAu film as described in Section 4.

The extent of Si diffusion into the thin film was studied by means of thicker Pd/Au films on Si wafer. In Fig. 7a and b, a series of XPS depth profile spectra are given for Au 4f and Pd 3d for a ∼121 Å PdAu film deposited on a ∼51 Å Si-oxynitride (SiO_xN_y) film grown on Si wafer. The characteristics of the Si-oxynitride are shown in Fig. 2c and d. The thickness of the PdAu film is determined using reflectivity, as presented below (Fig. 13). Here each cycle corresponds to ∼24 Å of material removal. In Fig. 8c the intensity (the area under the peak) of Pd, Au, and Si is shown versus the sputter cycle. In this figure we separate the silicide component of the Au 4f from the PdAu component by peak fitting in order to determine the position of the interface. Peak analysis of Au 4f indicates that the interface for this system is located roughly at cycle 7. This assignment is based on where the PdAu component of the Au 4f peak diminishes while the silicide component reaches a maximum. This is marked as a vertical dashed line in the figure. This assignment has uncertainties

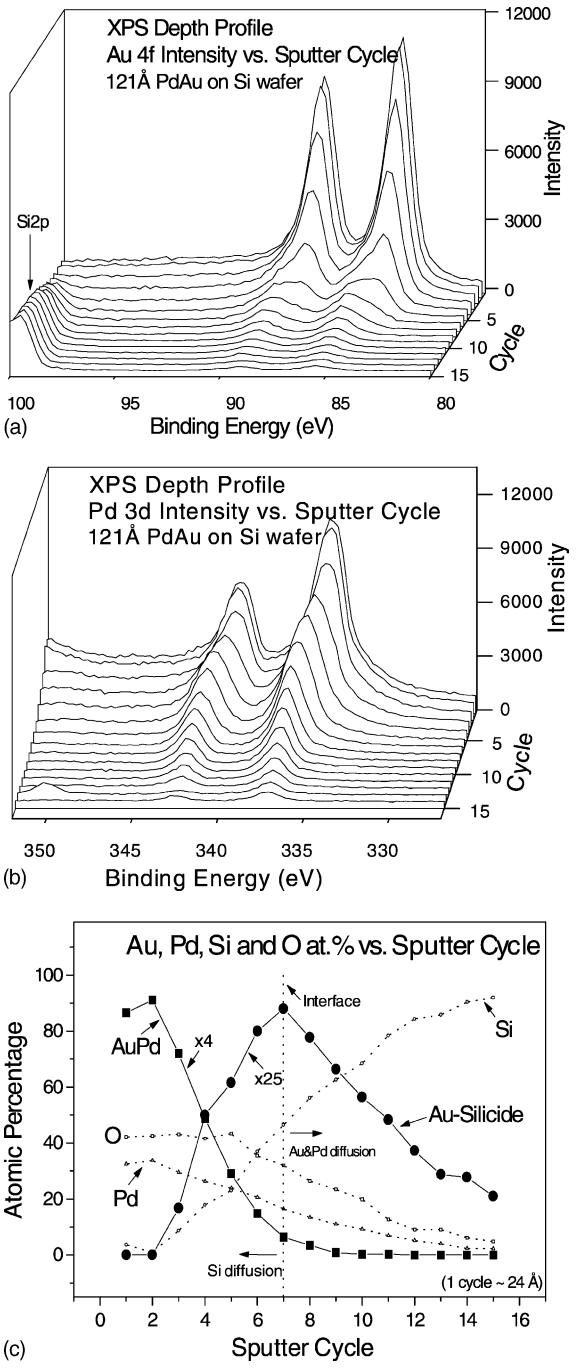

Fig. 8. (a) A montage of Au 4f vs. sputter cycle for a 121 Å AuPd film deposited on a ∼51 Å oxynitride film grown on a Si-wafer (see Fig. 2c and d). Also shown in the figure is Si 2p around the 100 eV binding energy, corresponding to the Si-bulk level; (b) a montage of Pd 3d vs. sputter cycle for the same film described in part (a). The interface is roughly at around cycle 7; (c) atomic percentage vs. sputter cycle for Au, Pd, Si and O. These are normalized so that the sum of all percentages at a given cycle add up to 100%. The Au 4f is separated into AuPd and Au-silicide components as described earlier. A vertical line is drawn roughly where the AuPd component of the Au concentration diminishes. Arrows mark the direction of the diffusion of Si, Au and Pd across the interface. A single cycle of sputtering is about 24 Å.

because of the attenuation lengths of electrons and because of the surface and interface roughness (including the sputter-induced roughness). The Au-silicide intensity has its maximum at the interface, as anticipated.

The silicide and PdAu components of the Pd 3d lines are not separated, though the interface at the 7th cycle was verified by comparing the peak profiles (see Fig. 8b) and peak positions (Fig. 9c). We also show the variation in the O intensity and the O 1s line as a function of sputter cycle in Fig. 8c and 9a, respectively. The sources of the oxygen signal are most likely the O trapped or absorbed in PdAu during and after film preparation and, in part, the Si-oxide and Si-oxynitride films on the substrate (see Figs. 7c and d and 8c). The Pd and Au may be interacting with such oxygen, causing a complicated mixture: this is supported by the behavior of the O 1s core line as a function of sputter cycle shown in Fig. 9a. Substantial core level activity is observed as a function of sputter cycle. The peak position shifts almost linearly by ∼1.7 eV to a higher binding energy. Compare this figure with Fig. 2b and d, where we observe a decrease in the binding energy of oxygen with increasing sputtering. This suggests that some fractions of Pd and Au participate in reactions in the oxide film. Meanwhile, the Au core levels corresponding to PdAu and Au-silicide phases remain more or less constant during sputtering, as shown in Fig. 9b, which is extracted from the data presented in Fig. 10a. On the other hand, Pd 3d behaves (Figs. 7b and 9c) very similarly to the O 1s line, which shifts toward the higher binding energy. In Fig. 9c the PdAu and Pd-silicide components are not separated. Our naive way to explain the observed behavior of O is to hypothesize that the O is dispersed at concentrations described in Figs. 5b, 6b and 8c in a mixture of multiple states involving partially oxidized PdAu film and SiO_xN_y and the Pd- and Au-silicides.

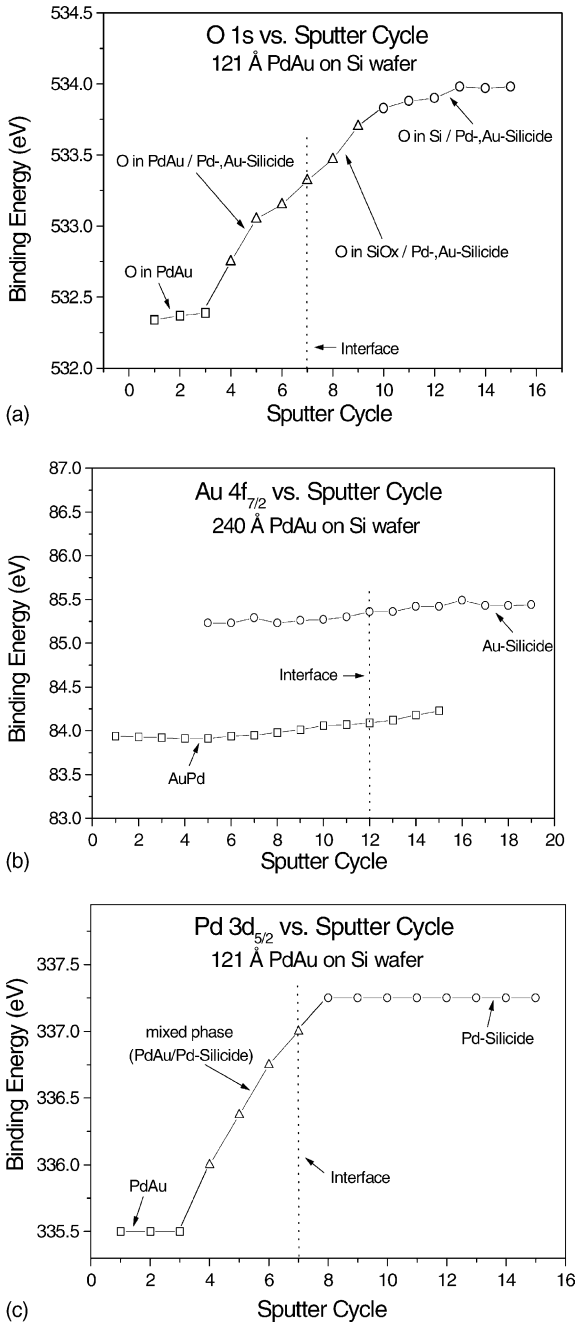

Fig. 9. (a) O 1s vs. sputter cycle for a 121 Å PdAu film described in Fig. 8. No attempt is made to separate the individual components of the O 1s line. The figure suggests that O is interacting with PdAu film when compared with Fig. 2b and d (see text for details): in early stages of sputtering the oxygen is most likely described as environmentally chemisorbed O in PdAu in the presence of low concentration silicides; as we approach the interface oxygen will be mostly be associated with the SiO_x phase intermixed with a small concentration of silicides. As the sputtering proceeds oxygen will be in an environment mostly surrounded by Si and silicides. These are symbolically marked on the figure in relation to the interface; (b) Au $4f_{7/2}$ vs. sputter cycle for the sample described in Fig. 10a. Notice that peak positions are insensitive to sputter cycle and vary very slowly with increasing sputtering. The position at ~85.3 eV is attributed to Au-silicide and that at ~84 eV to Au in AuPd phase. The peak fittings were done similar to that shown in Fig. 5a; (c) Pd $3d_{5/2}$ vs. sputter cycle for the thin film described in Fig. 8. No attempt was made to separate the peak into PdAu and Pd-silicide components because of the lack of reliability. Only the average peak position is shown as a function of sputter cycle. The system goes through a mixed phase consisting of PdAu and Pd-silicide and gradually becomes pure Pd-silicide as marked on the figure.

The surprising result of this study is how far a small fraction of Si has diffused into the PdAu film: as observed for the 46 and 121 Å films (Figs. 5b, 6b, and 8c, respectively), the Si diffuses almost to the top of the PdAu films; for the 121 Å film this is a displacement of more than 100 Å. In this analysis the electron attenuation and penetration depths are not taken into account, which can explain some of the Si signal but not all. As mentioned above, both the Pd and Au diffuse into the bulk Si by first going through the oxide film. This is visible in Fig. 8a, where the bulk Si 2p core level at around 100 eV is also visible. Notice that traces of Pd and Au are visible ~200 Å below the interface. Coupling this with the chemical shifts in the Au 4f and Pd 3d levels suggests that the surface and interface roughness is not enough to explain our observations on the Pd and Au diffusion into the Si bulk. A concept of *chemical* roughness needs to be invoked.

In order to determine the maximum distance of Si diffusion into the PdAu film we deposited a ~240 Å PdAu film on a ~43 Å Si-oxynitride grown on a Si substrate, similar to that described in Fig. 2c and d. The XPS depth profile is given in terms of Au 4f and Pd 3d versus the sputter cycle in Fig. 10a and b. Here, too, each cycle corresponds to ~24 Å depth. Fig. 10c shows the atomic concentration versus the sputter cycle for Pd 3d, Au 4f (split into two) and Si 2s. The behavior of the peak positions is consistent with the observations for the thinner films. The interface is marked as a vertical dashed line at about the 12th cycle in Fig. 10c. AFM images suggest that the PdAu films are continuous with surface roughness better than 20 Å. The usual uncertainties in electron attenuation

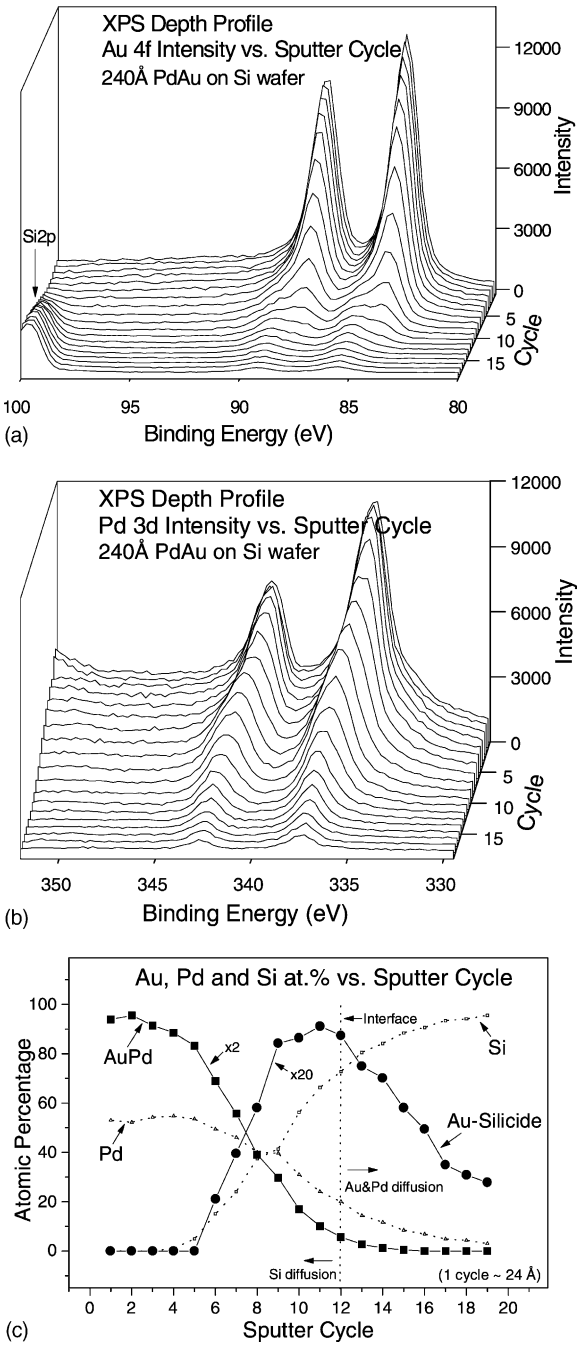

Fig. 10. (a) Montage of Au 4f intensity vs. sputter cycle for a 240 Å PdAu film deposited on a 43 Å oxynitride film (very similar to that described in Fig. 2c and d) grown on a Si-wafer. The features around 100 eV show the bulk Si 2p as a function of sputter cycle. Note that cycle 12 is marked as the interface, where the PdAu is reduced to ∼5% of its maximum; here, we assume that length and surface and interface roughness make the interface determination uncertain by at least ±1 cycles, or ∼ ±25 Å.

Notice that (Fig. 10c) Si penetrates as much as ∼170 Å into the PdAu film: this is most likely the upper limit for Si penetration into a PdAu substrate. It is, however, very interesting that Au-silicide intensity decreases very rapidly as one approaches the PdAu surface. The majority of Si atoms in this region are associated with the oxide layer. Furthermore, the silicide formation is, as before, maximum around the interface, and the Pd and Au penetrate into the Si substrate by more than 200 Å.

3.2. Angular dependence

Is the Si really moving towards the surface? Is the oxide layer participating in silicide reactions? Does Ar-ion bombardment cause any of the chemical reactions we observe? One of the best non-invasive depth profile methods to answer such questions is angular-dependent photoemission spectroscopy [38]. Though this method has a limited range (thickness) of applications, the information gathered represents the true chemical and physical state of the interface. This is because the surface is not subjected to particle beam damage. To shed light on some of the intriguing questions, results of an angular-dependent XPS are presented in Fig. 11, where the angular-dependent atomic concentrations of C, O, Si, Pd and Au for ∼15 Å PdAu film on a ∼82 Å oxide layer grown on a Si substrate are plotted as a function of electron emission angle. A period of ∼2 months elapsed between the preparation of the thin film and the XPS analysis. The film has been subjected to hours of Cu Kα radiation in ambient conditions for

some of the interface broadening is induced by Ar-ion bombardment (see [46]); (b) Pd 3d intensity vs. sputter cycle for the same film described above. Note that Pd silicide dominates after cycle 12; (c) atomic concentrations of Pd, Au and Si for the system described above as a function of sputter cycle. The concentrations are normalized to yield 100% when the Au, Pd and Si concentrations at a given cycle are added together. The Au concentrations are separated into individual components of AuPd and Au-silicide as discussed in the text (see Fig. 5). The vertical dashed line marks the interface within the accuracy of our experimental limitations. Horizontal arrows show the direction of Si, Au and Pd diffusion. No attempt is made to separate the individual components of Pd 3d peaks.

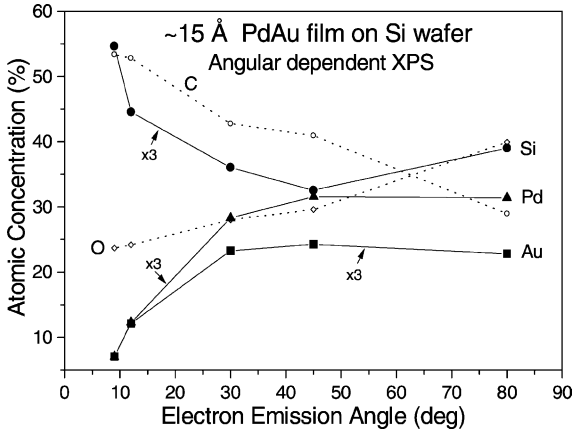

Fig. 11. Atomic concentration of C, O, Si, Pd and Au vs. angle of emission of the photelectrons for a ∼15 Å PdAu film deposited on a ∼ 82 Å Si-oxide film grown on a Si-wafer. Atomic concentrations are normalized to add up to 100% at each angle. Note that Si (and C) dominates at grazing emission angles, signifying high surface concentrations.

reflectivity studies. The angular acceptance of the analyzer was ±7°. Though this is not an optimum angular resolution the observed trend of variation in concentrations is rather informative and supportive of the sputter depth profile analysis presented above. Notice, for example, that the Pd and Au increase nonlinearly with increasing angle and reach saturation above 30° emission. On the other hand, the O concentration increases almost linearly while the C concentration decreases in a similar fashion. The most interesting behavior is the Si concentration: first it decreases nonlinearly and reaches a broad minimum around 45°; then it increases slowly until it reaches near-normal emission. Considering that any atomic species concentrated on the surface will show a high peak intensity at the grazing angle of emission, the Si and C appear to fit this profile. The C is an environmental contaminant and is expected to be concentrated on the surface. It is expected to decrease with increasing emission angle because it is mostly concentrated on the surface (e.g. see Fig. 2a and c). However, the behavior of the Si is rather surprising. The sharp drop in Si concentration with increasing angle suggests a high concentration of Si on the very top of the surface; its subsequent increase with increasing emission angle is also consistent with the high concentrations of Si which exist below the thin film because of the presence of the substrate. This observation suggests that the Si penetrated through ∼15 Å of thin film and is residing on the very top of the film. Such behavior has been reported in the literature [12]; in our case the most likely source of Si is the thick (∼82 Å) Si oxide film itself. The fact that the O increases linearly with increasing angle is not surprising because of the thick Si oxide layer located between the thin film and the substrate. In Section 4 below the core level data related to Fig. 11 are presented, giving further evidence for the conclusions reached here.

3.3. Reflectivity studies

As evident in the above presentation, a complicated interface forms when a layer of PdAu alloy is deposited on Si-oxide or Si-oxynitride grown on a Si wafer. We conducted X-ray reflectivity studies on these films to better understand them in terms of their thickness, density, roughness and perhaps even interface formation.

In Fig. 12, we show the specular reflectivity versus angle of incidence corresponding to the XPS data presented in Figs. 3 and 4. The full circles represent the actual measurements, while the full line shows the theoretical fit performed using the "*X-ray interaction with matter*" program on the Lawrence Berkeley Laboratory web site at http://www-cxro.lbl.gov. A bilayer model is used in which the first layer is made up of Pd and Au atoms at a uniform density, and the

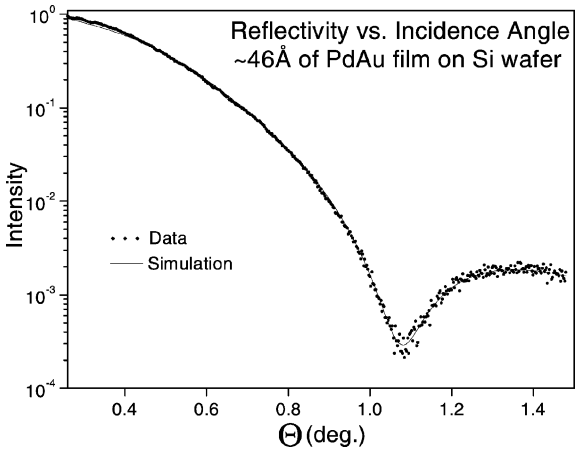

Fig. 12. Reflectivity vs. incidence angle for the 46 Å PdAu film as described in Figs. 3–7. The dotted line shows the actual data and the full line is the bilayer-model fit as described in the text.

second layer is a mixture of Pd, Si, O and Au having slightly more density than Si with physical roughness at all sides. The agreement is rather good and the theoretical fit suggests that the thickness of the film is ∼46 Å accurate to less than 1 Å, and that the surface and interface roughnesses are ∼4 Å. The density of the film is about 13 ± 1 g/cm^3. The theory is not very sensitive to the second-layer properties, which in this case represent a thickness of ∼60 Å with a density of ∼3.4 g/cm^3 and a surface roughness of ∼4 Å. In the model this layer is situated between the Si substrate and the PdAu film. This system is also modeled as a single layer ignoring the second layer totally: it is found that the AuPd parameters (thickness and density) are nearly the same as in the bilayer model and that these values are not sensitive to the existence or lack of the second layer. Therefore, the only reliable information that can be obtained from our reflectivity studies are the film thickness and the densities of the PdAu films. The rest of the information is model-dependent and is not acceptable.

In Fig. 13, the theoretical and experimental comparisons of the reflectivity are given for a thicker layer of PdAu alloy. This figure is related to the XPS depth profiles shown in Fig. 8a and b. Both the single- and bilayer-model fits are tested, and the results do not show an appreciable difference in terms of first-layer thickness or density. The thickness of the film is about 121 Å, accurate to 1 Å or less. The surface and interface roughnesses of the first layer are about 6 and 10 Å, respectively. As stated above, the quality of the fit is less sensitive to the second-layer parameters in that the density is ∼3.4 g/cm^3 and the thickness ∼120 Å. In our studies the XPS depth profiles are a better representation of the interface analysis than those obtained from reflectivity. Off-specular reflectivity coupled with more sophisticated data analysis will improve the reliability of the data pertaining to the interface properties.

The thickest film we studied with reflectivity is shown in Fig. 14. The data suggest that the density of the film is about 12 g/cm^3 and that the thickness is about 240 Å. The surface and interface roughnesses are about 9 and 10 Å, respectively. As before, the second-layer parameters do not change the density and thickness determined above. In this particular case the density of the second layer is about 4.2 g/cm^3 and its thickness is about 240 Å. In all of these studies 2.33 g/cm^3 is used for the Si substrate density.

In order to restore our confidence in the reflectivity results, a layer of pure Au film was deposited, using procedures identical to those described above, on a ∼46 Å Si-oxide layer grown on a Si wafer. The theoretical fit using the bilayer model gave a density of 18.2 g/cm^3 and a thickness of ∼175 Å. The top layer and interface roughnesses were 4 and 13 Å, respectively. As before, the film thickness and the density were insensitive to the second-layer properties. A mass density of 18.2 g/cm^3 means that the deposition produced a defect density of ∼5.7% of the ideal packing. Besides uncertainties in determining

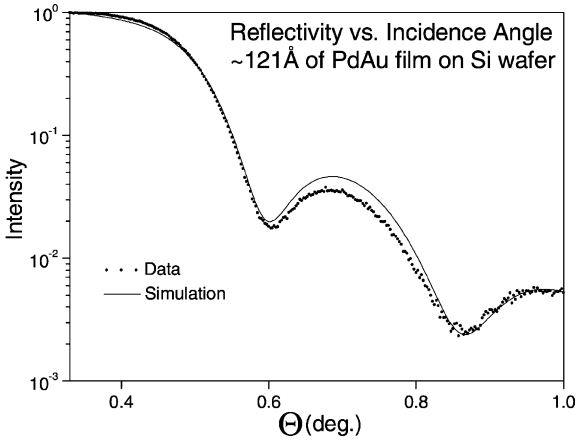

Fig. 13. Reflectivity vs. the incidence angle for the 121 Å PdAu film on a Si-wafer described in Figs. 8 and 9a and c. The dotted line is the actual data and the full line is the bilayer-model fit.

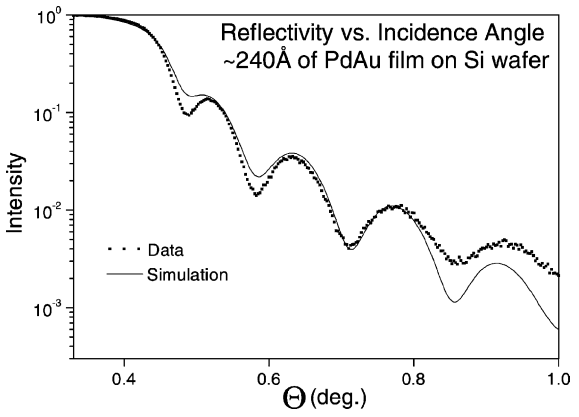

Fig. 14. Reflectivity vs. the incidence angle for the 240 Å PdAu film on a Si-wafer described in Figs. 9b and 10. The dotted line is the actual data and the full line is the bilayer-model fit.

the mass density which could be as much as 1 g/cm^3, other factors that contribute to the apparent defect density will include but are not limited to non-flat (grainy) topography, trapped gasses in the film, and the actual defects formed during deposition.

3.4. Thin-film diffraction studies

Thin-film diffraction studies were conducted to determine the crystal structure of the thin films and that of the interlayer. Fig. 15 shows a montage of grazing incidence X-ray diffraction spectra as a function of the incidence angle for the thick (∼240 Å) Pd/Au film described in Figs. 10a and b and 14. The angle of incidence of the Cu Kα X-rays varied from $\Omega = 0.2^\circ$ to 2.0° (Fig. 1). The relative intensities of the peaks related to the thin film and those related to the substrate changed as a function of the angle of incidence, as anticipated. The peaks around $2\theta = 39^\circ$ and 45° are assigned to the (1 1 1) and (2 0 0) diffraction peaks belonging to the PdAu alloy, while the peak around $2\theta = 53^\circ$ belongs to the Si(3 1 0) diffraction line. The features around $2\theta = 56^\circ$ are associated with the Si substrate (such as the (3 1 1) lines, which were not expected to be strong because of the single crystal nature of the Si(1 0 0)). These peaks were confirmed by running thin-film diffraction on the Si substrate without PdAu film. Furthermore, thin-film diffraction studies were conducted on the pure Au film deposited on the Si substrate, and the results confirmed the expected diffraction pattern, similar to that shown in Fig. 15: the Au(1 1 1) line appeared at about $2\theta = 38^\circ$, and the Au(2 0 0) line appeared at about $2\theta = 44^\circ$, with the intensity ratios as documented by the diffraction libraries. Careful analysis of the diffraction data of the PdAu film suggests that the lattice parameter of the film is 4.004 ± 0.014 Å. This falls between the values of 4.08 Å for Au and 3.89 Å for Pd. The Pd and Au atoms randomly occupy the face-centered cubic (fcc) sites of a cubic structure. The mass density of a hypothetical thin film corresponding to an ideal packing can easily be determined by making use of XPS quantitative analysis. The Au to Pd concentrations in cycle 1 are determined to be about 47.5 and 52.5%, respectively; hence, Pd_xAu_{1-x}, $x = 0.53$. Taking into account the measured lattice parameter and the statistical distribution of the Pd and Au atoms placed on the lattice site (with an average mass of 149.43 amu) gives an ideal density of 15.5 g/cm^3. This value is substantially larger than the 13 ± 1 g/cm^3 measured in our films. This result is consistent with the XPS determinations, where not only the pure PdAu phase but also the Pd- and Au-silicides as well as C and O are all mixed into the matrix of the thin film (see Fig. 8c and 11). These all contribute to the reduction of the mass density. Other factors that contribute to the apparent reduction in the mass density are the non-flat (grainy) film structure and actual vacancies introduced during thin film deposition. Hence, the thin-film diffraction and XPS results are consistent with each other.

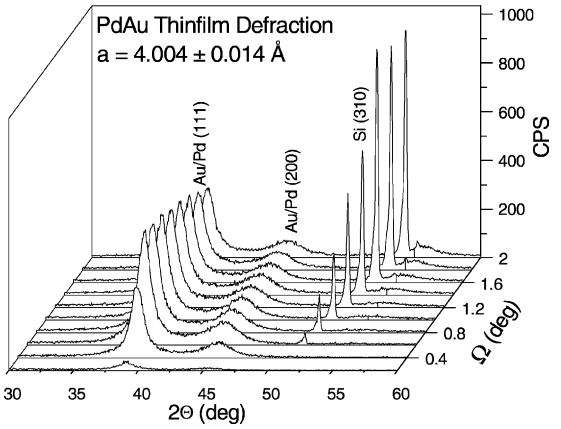

Fig. 15. Montage of grazing X-ray diffraction vs. 2θ for the sample described in Fig. 14 as a function of angle of incidence, Ω, varying from 0.2° to 2° in steps of 0.2°. The peak positions related to the thin film are assigned to AuPd (1 1 1) and AuPd(2 0 0) diffraction beams as shown in the figure. The major substrate-related peak is identified as Si(3 1 0) in the figure. The minor features above Si(3 1 0) are also related to the substrate, which is verified by running a grazing incidence X-ray diffraction spectrum on a bare Si-wafer. It is also clear that these features grow with increasing angle of incidence, Ω, indicating that the features are related to the Si(1 0 0)-wafer.

4. Discussion

Our observations suggest that the AuPd/dielectric film/Si(1 0 0) system forms a reactive interface. It appears that this reactive interface takes place in spite of the reasonably thick (40–50 Å) dielectrics of

Table 1
Comparison of the peak positions and FWHMs of Si, Au, Pd and C for 9° and 80° emission angles[a]

Angle (°)		Atom			
		Si 2p	Au 4f	Pd 3d	C 1s
9	Peak position (eV)	102.3	84.3	336.3	284.9
	FWHM (eV)	1.67	1.45	2.75	1.68
80	Peak position (eV)	103.4	84.3	335.8	284.9
	FWHM (eV)	2.57	1.26	2.30	1.64

[a] These data correspond to Fig. 11.

Si-oxide or Si-oxynitride grown on Si. Such dielectrics are not able to form a diffusion barrier against the migration of Si into PdAu film or of Pd and Au into Si bulk. In fact, the data suggest that the oxide layer actively participates in the reactions. It is not clear what the microscopic nature of these reactions are in these dynamic and reactive processes.

Sputtering a surface is a destructive process, both physically and chemically. Is it possible that Ar bombardment causes some of the observed interdiffusion and chemical changes? It is well known, for example, that ion bombardment causes differential etching, surface roughening, and enhanced interdiffusion. For example, Bukaluk [46] reports the effects of Ar-ion sputtering on degradation of depth resolution as a result of interdiffusion in thin films of bi- and multi-layer Pd/Au systems. Most of these effects are visible after 300 Å of profiling. We admit that some of these effects are inescapable and are present in our data (Fig. 10). However, their contribution is mostly neglected in our analysis. Experimentation with 3.5 and 2 keV Ar-ion beam energies on the same system did not yield different results. It would be difficult to explain the Si signal in the XPS studies of PdAu thin film ∼170 Å before the interface being caused as a result of ion bombardment! The formation of PdAu islands will explain the latter observation but AFM studies do not agree with this assessment. The charge state of Pd and Au may be affected by Ar-ion bombardment; hence, some of the peak shifts might be attributed to beam damage. However, our current belief is that the observed interfaces are formed during and after the deposition and perhaps are even aided by Cu Kα radiation during reflectivity and diffraction studies, and we have no convincing evidence contrary to this hypothesis. The migration of Si into thick gold films and silicide formations in Au/Si and Pd/Si interfaces under ambient conditions has already been reported in the literature [12,19,20], which gives support to our current view of the PdAu/Si-oxide/Si interface.

As discussed earlier, the angular-resolved XPS presented in Fig. 11 support the idea that the Si is migrating from the substrate to the top of the ∼15 Å AuPd film. This idea is further supported by the peak positions and FWHMs of Si, C, Au and Pd compared at two extreme angles of emission, 9° and 80° (near normal emission). This is shown in Table 1.

The Au 4f and Pd 3d levels are shown as references. The main issue is the behavior of the Si 2p level relative to the other peaks, particularly to C 1s, which is usually accepted as the reference position in such comparisons [47]. Note that at the 9° emission angle Si 2p is positioned at ∼102 eV and its FWHM is about 1.67 eV, while at the 80° emission angle Si 2p is positioned at ∼103.4 eV and its FWHM is about 2.57 eV. The explanation for these observations is that at grazing emissions spectra are sensitive to the top-layer atoms of the surface, so that the Si 2p state is expected to be substantially different from the Si 2p inside the Si-oxide layer. Hence, at grazing emissions a nearly pure state of Si is observed on top of the surface, while at near-normal emission both states are visible to the detector, so that two peaks with ∼1 eV separation yield a broader peak at a different position, as observed in the experiment. Notice that the C 1s peak properties do not change much with the varying angle of incidence. Notice also that the Pd 3d position at ∼336.3 eV is shifted by ∼1 eV from 335.3 eV for the pure PdAu; meanwhile a small shift (∼0.3 eV) is observed in Au 4f. This is interpreted as the Si atoms on the surface interacting predominantly with the Pd atoms rather than with the Au atoms.

In Fig. 7d, it appears that the locations of the PdAu and SiO_2 layers are superimposed on each other. This apparent paradox can be easily resolved if one compares Fig. 7a and b with Fig. 7c, where it is clearly seen that the oxide layer extends beyond the interface. The apparent oxide signal within the PdAu film is due in part to the finite attenuation length of the photoelectrons produced inside the Si-oxide layer, traversing the PdAu film on the way to the analyzer, and in part to the O from air trapped in PdAu film during or after deposition. Hence, the data are consistent with the expected layer geometry.

The temporal properties of the diffusion, reaction and interface formations of these systems have not been investigated. The minimum time between thin-film preparation and XPS analysis was about 2 months. Samples were exposed to Cu Kα X-rays continuously for hours at a time during analysis, and they were kept in ambient atmosphere. As mentioned above the physical roughnesses of the substrates are typically less than 5 Å and those of the thin films are about 10–15 Å, as determined by the AFM measurements. The formation of silicides and related interdiffusion near the interface as well as the formation of physical roughness might be influenced by the above factors (time and exposure to X-rays).

The X-ray reflectivity suggests a reasonably sharp boundary with considerable differences between the densities of the thin film and those of the substrate, as presented in Section 3.3 above. The depth profile of the Si-oxide layer in PdAu film behaves slightly differently in terms of Si 2p analysis (Fig. 7c and d) than that of the Si-oxide layer without PdAu film, as shown in Fig. 2a and b. The differences are attributed to interaction of the PdAu film with the oxide or oxynitride layer of the substrate. X-ray reflectivity is a very accurate way to determine the average film thickness, which is separated by sharp mass density from that of the substrate. The thickness measurements were also confirmed using sputter-rate calibrations of the XPS Ar-ion gun as well as AFM. Both the PdAu film thickness and the Si-oxide thickness, each ∼46 Å, are rather accurately determined. The data indicate that only small fractions of the available Si, Au, and Pd have participated in silicide reactions as presented earlier.

Other evidence suggesting that PdAu interacts with the oxide or oxynitride layer is seen in the comparison of the O 1s core position as a function of the sputter cycle shown in Fig. 9a and that shown in Fig. 2b. Ordinarily the sputter process causes the O 1s level to shift down by about 1 eV when no PdAu is present (Fig. 2b), while the same process as shown in Fig. 9a produces an opposite behavior, an upward shift of ∼1.7 eV when the PdAu is deposited on the oxide. Some of the oxygen in the thin film is incorporated into the film during and after the film preparation. This means O either from air or from the Si-oxide is interacting with the Pd and Au species, all of which mix and interact as a result of the diffusion of Si, Pd, Au and even O into each others' regions.

Whether or not the N was present in the Si-oxide film did not make any difference in the diffusion and reactive processes between the PdAu and the substrate, even though the N in Si-oxide or Si_3N_4 films on Si substrate was known to strengthen the diffusion barrier properties (against boron) as well as prevent leakage and electric breakdown in the thin oxide films in microelectronic device technology [48,49]. A depth profile analysis of the Si-oxynitride film is very similar to that of the Si-oxide film (Fig. 2). The chemical nature of an oxynitride matrix is discussed in [39]. As shown, however, in Figs. 8–10 the diffusion and reaction processes of PdAu on Si-oxynitride are very similar to those observed with a PdAu film on a thick Si-oxide film. The role of the N is totally ignored in our analysis.

Our observations suggest a silicide interface, whose FWHM, extracted from the Au-silicide versus sputter cycle curves shown in Figs. 5b, 6b, 8c and 10c, seems to depend on the film thickness. It is determined that the FWHMs of the silicide formations in 46, 121 and 240 Å films are 70, 180 and 220 Å, respectively. The thickness dependence of this reactive interface seems to correlate with Si diffusion into the thin films as shown in Figs. 5b, 6b, 8c and 10c, where the Si diffusion measured from the interface is ∼45, 120 or 170 Å for 46, 121 or 240 Å PdAu films, respectively.

The nature of the diffusion process is obviously complicated, particularly in the systems studied here. In [7,8] a mass-exchange mechanism is suggested for the dynamic process involving Si and Au interdiffusion. A similar mechanism can be considered for Au and Pd diffusion into Si oxide, though at this time all of these ideas are speculative. Experimentally, the

accumulation of Pd in the Si oxide appears to be greater than that of Au. In general, the thermodynamical conditions that can give rise to such a situation involve complicated chemical potential gradients for Pd, Au, O, N and Si. These are established across the interface upon deposition of the PdAu thin films in such a way that the equilibrium condition is established when the constituent atoms diffuse and react with each other to form a reactive interface as described above. Ion beam induced atomic transport is addressed in the reference [50], where an 80 keV Ar^+ beam is allowed to interact with the Pd/Au bilayer. The conclusions of reference [50] are not directly applicable to our results.

No evidence of crystallinity is observed for the Au- and Pd-silicide in the grazing-incidence X-ray diffraction (XRD) data. It is most likely that such reactions produce amorphous structures as reported in [11], which is an even stronger probability in our case because of the involvement of the amorphous Si-oxide and Si-oxynitride structures in the silicide formations. Also, the concentrations of these silicides in the interface might be outside the detection limit of our XRD system.

5. Conclusions

Several very interesting features of PdAu films have now been brought to light: PdAu films on a 40–50 Å oxide or oxynitride dielectric grown on a Si wafer form a reactive interface. The major fraction of the film is an fcc structure with a lattice constant of 4.004 ± 0.014 Å and a thin-film density of 13 ± 1 g/cm^3. The ideal density of the Pd_xAu_{1-x} ($x \sim 0.53$) film is expected to be about 15.5 g/cm^3. This means the film has a substantial amount of defects as well as light Si, O, N and C impurities in it. A reactive interface is formed in which the thin-film Pd and Au atoms and substrate Si atoms are diffused into the opposite regions. This way a reactive interlayer consisting of Au- and Pd-silicide extending into and mixing with the PdAu and Si-oxide or Si-oxynitride is established. The concentration versus depth of the silicide has a maximum at the PdAu interface and decays rapidly on both sides of the interface. The FWHM of this profile saturates at ~220 Å for ~240 Å PdAu film. For thinner films the FWHM is reduced and is regulated by the diffusion of Si into the PdAu thin film. It is clear that PdAu films interact with the Si-oxide or Si-oxynitride films but the microscopic nature of this interaction is not yet clear. Finally, silicides established in the interface region appear to be amorphous. No attempt was made to characterize the temporal evolution of these interfaces in the 2-month period between the time they were prepared and the time they were analyzed using XPS depth profiling.

Acknowledgements

This work was supported by funds from the Image and Chemical Analysis Laboratory (ICAL) at MSU, and one of us (S.Y.) is indebted for the sabbatical leave support he received from Bahcesehir University in Istanbul, Turkey. The authors greatly appreciate the help received from Ms. Ayca Yalcin of Bilkent University in Ankara, Turkey, Dr. Jim Anderson, Mr. Marcus Teter, Mr. Chad Bohannan, Ms. Angie Cheff and the ICAL staff (at Montana State University in Bozeman), and the valuable discussions with Prof. Dick Smith and Prof. Jerry Lapeyre (of MSU Physics) during the course of this work. Finally, the editorial help of Mrs. Lois Avci is greatly appreciated.

References

[1] A. Sarkany, A. Horvath, A. Beck, Appl. Catal. A: Gen. 229 (2002) 117.
[2] S.N. Reifsnyder, H.H. Lamb, J. Phys. Chem. 103 (1998) 321.
[3] W. Juszczyk, Z. Karpinski, D. Lomot, J.J.W. Sobczak, J. Catal. 151 (1) (1995) 67.
[4] T.J. Schimid, Z. Jusys, H.A. Gasteiger, R.J. Behm, U. Endruschat, H. Boennemann, J. Electroanal. Chem. 501 (2001) 132.
[5] J.I. Goldstein, D.E. Newbury, P. Echlin, D.C. Joy, J.A.D. Romig Jr., C.E. Lyman, C. Fiori, E. Lifshin, Scanning Electron Microscopy and X-Ray Mircroanalysis, 2nd ed., Series, Plenum, New York, 1992.
[6] C. Grupp, A. Taleb-Ibrahimi, Phys. Rev. B 57 (1998) 6258.
[7] H. Minoda, K. Yagi, Phys. Rev. B 60 (1999) 2715.
[8] H. Minoda, K. Yagi, F.-J.M.Z. Heringdorf, A. Meier, D. Kahler, M.H.V. Hoegen, Phys. Rev. B 59 (1999) 2363.
[9] F.-J.M.Z. Heringdorf, T. Schmidt, S. Heun, R. Hild, P. Zahl, B. Ressel, E. Bauer, M.H.-V. Hoegen, Phys. Rev. Lett. 86 (2001) 5088.
[10] M. Shibata, I. Sumita, M. Nakajima, Phys. Rev. B 57 (1998) 1626.

[11] C.R. Chen, L.J. Chen, Appl. Surf. Sci. 92 (1996) 507.
[12] L.A. Gheber, M. Hershfinkel, G. Gorodetsky, V. Volterra, Thin Solid Films 320 (1998) 228.
[13] I.V. Lyubinetsky, V.K. Adamchuk, Thin Solid Films 288 (1996) 182.
[14] I. Chizhof, G. Lee, R.F. Willis, Phys. Rev. B 56 (1997) 12316.
[15] B. Sundaravel, K. Sekar, G. Kuri, P.V. Satyam, B.N. Dev, S. Bera, S.V. Narasimhan, P. Chakraborty, F. Caccavela, Appl. Surf. Sci. 137 (1999) 103.
[16] E. Landree, D. Grozea, C. Collazo-Davila, L.D. Marks, Phys. Rev. B 55 (1997) 7910.
[17] J.F. Chen, L.J. Chen, Mater. Chem. Phys. 39 (1995) 229.
[18] C.J. Ennis, D.J. Spence, S.P. Tear, E.M. McCash, Phys. Rev. B 61 (2000) 8443.
[19] E. Kampshoff, N. Walchli, K. Kern, Surf. Sci. 406 (1998) 117.
[20] E. Kampshoff, N. Walchli, K. Kern, Surf. Sci. 406 (1998) 103.
[21] N. Walchli, E. Kampshoff, A. Menck, K. Kern, Surf. Sci. 382 (1997) 705.
[22] W.E. Wallace, W.L. Wu, Appl. Phys. Lett. 67 (1995) 1203.
[23] T.P. Russel, Mater. Sci. Rep. 5 (1990) 171.
[24] C.A. Lucas, T.D. Nguyen, J.B. Kortright, Appl. Phys. Lett. 59 (1991) 2000.
[25] C.A. Lucas, P.D. Hatton, S. Bates, T.W. Ryan, S. Miles, B.K. Tanner, J. Appl. Phys. 63 (1988) 1936.
[26] S.M. Heald, B. Nielsen, J. Appl. Phys. 72 (1992) 4669.
[27] S. Santucci, A.V.L. Cecilia, A.R. Phani, R. Alfonsetti, G. Moccia, M.D. Biase, Appl. Phys. Lett. 76 (2000) 52.
[28] M.F. Toney, S. Brennan, J. Appl. Phys. 66 (1989) 1861.
[29] C. Thompson, G. Palasantzas, Y.P. Feng, S.K. Sinha, J. Krim, Phys. Rev. B 49 (1994) 4902.
[30] B. Cull, Y. Shi, S. Kumar, R. Shih, J. Mann, Phys. Rev. E 51 (1995) 526.
[31] R.P. Chiarello, H. You, H.K. Kim, T. Roberts, R.T. Kempwirth, D. Miller, K.E. Gray, K.G. Vandervoort, N. Trivedi, S.R. Phillpot, O.J. Zang, S. Williams, J.B. Ketterson, Surf. Sci. 380 (1997) 245.
[32] B.E. Koel, A. Sellidj, M.T. Paffett, Phys. Rev. B 46 (1992) 7846.
[33] http://www.physics.montana.edu/ical/ical.html.
[34] N. Miyata, H. Watanabe, M. Ichikawa, Phys. Rev. B 58 (1998) 13670.
[35] Y. Yamashita, A. Asano, Y. Nishioka, H. Kobayashi, Phys. Rev. B 59 (1999) 15872.
[36] A. Stesmans, G.V. Gorp, Phys. Rev. B 39 (1989) 2864.
[37] A. Stesmans, G.V. Gorp, Phys. Rev. B 52 (1995) 8904.
[38] J.H. Oh, H.W. Yeom, Y. Hagimoto, K. Ono, M. Oshima, N. Hirashita, M. Nywa, A. Toriumi, A. Kakizaki, Phys. Rev. B 63 (2001) 205310.
[39] G.F. Cerefolini, A.P. Caricato, L. Meda, N. Re, A. Sgamellotti, Phys. Rev. B 61 (2000) 14157.
[40] P. Aubert, H.J.V. Bardeleben, F. Delmotte, J.L. Cantin, M.C. Hugon, Phys. Rev. B 59 (1999) 10677.
[41] G.-M. Rignanese, A. Pasquarello, Phys. Rev. B 63 (2001) 75307.
[42] http://www.anatechltd.com/pdf/hum6.pdf.
[43] R. Avci, J. Anderson, 2003, to be submitted for publication.
[44] Z.H. Lu, J.P. McCaffrey, B. Brar, G.D. Wilk, R.M. Wallace, L.C. Feldman, S.P. Tay, Appl. Phys. Lett. 71 (1997) 2764.
[45] P.J. Cumpson, M.H. Seah, Surf. Interf. Anal. 25 (1997) 430.
[46] A. Bukaluk, Appl. Surf. Sci. 175–176 (2001) 790.
[47] P. Swift, Surf. Interf. Anal. 4 (1982) 47.
[48] J.W. Klaus, A.W. Ott, A.C. Dillon, S.M. George, Surf. Sci. 418 (1998) L14.
[49] S.C. Song, H.F. Luan, C.H. Lee, A.Y. Mao, S.J. Lee, J. Gelpey, S. Marcus, D.L. Kwong, Microelectron. Eng. 48 (1999) 55.
[50] G.S. Chang, S.M. Jung, J.H. Song, H.B. Kim, J.J. Woo, D.H. Byun, C.N. Wang, Nucl. Instrum. Meth. Phys. Res. B 121 (1997) 244.